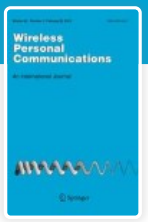

Wireless Personal Communications

An International Journal

Editorial board Aims & scope Journal updates

Wireless Personal Communications is an archival, peer reviewed, scientific and technical journal addressing mobile communications and computing. It investigates theoretical, engineering, and experimental aspects of radio communications, voice, data, images, and multimedia. — show all

Editor-in-Chief
Ramjee Prasad

Publishing model
Hybrid (Transformative Journal). How to publish with us, including Open Access

2.017 (2021)
Impact factor

1.563 (2021)
Five year impact factor

204 days
Submission to first decision (Median)

566,135 (2021)
Downloads

Latest issue

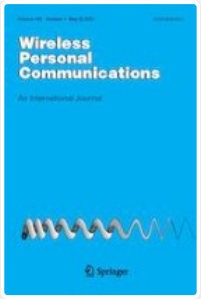

Volume 130

Issue 1, May 2023

View all volumes and issues >

Latest articles

Analysis of the Phase Velocities of (Pure, Slow and Fast) Alfvèn Waves in the E Region of the Ionosphere for Low Latitudes

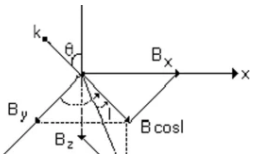

Kadri Kurt

OriginalPaper | Published: 01 May 2023

Quad Element Beamforming Microstrip Antenna for Indoor User Equipment Localization at 6 GHz Band

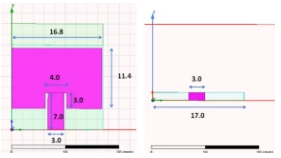

G. Thirunavukkarasu, G. Murugesan ... S. Kowsikkumar

OriginalPaper | Published: 01 May 2023

New Electronically Tunable Four-Quadrant Analog Multiplier Employing Single EXCCCII and Its Applications

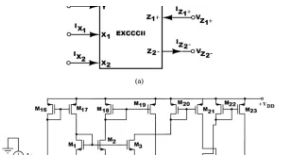

Rupam Das & Shireesh Kumar Rai

OriginalPaper | Published: 29 April 2023

Design and Implementation of Power-Efficient Cryptography Scheme Using a Novel Multiplication Technique

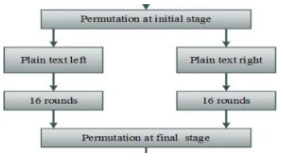

B. Srikanth, J. V. R. Ravindra ... D. Ajitha

OriginalPaper | Published: 28 April 2023

A Novel Hybrid Protocol in Achieving QoS Regarding Data Aggregation and Dynamic Traffic Routing in IoT WSNs

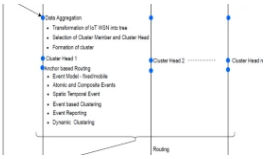

Neeraj Chandnani & Chandrakant N. Khairnar

OriginalPaper | Published: 28 April 2023

This journal has 177 open access articles

View all articles >

Journal updates

COVID-19 and impact on peer review

As a result of the significant disruption that is being caused by the COVID-19 pandemic we are very aware that many researchers will have difficulty in meeting the timelines associated with our peer review process during normal times. Please do let us know if you need additional time. Our systems will continue to remind you of the original timelines but we intend to be highly flexible at this time.

Call for Papers

A full list of all current calls for papers and open special issues is available.

View all updates >

For authors

Submission guidelines

Manuscript editing services

Ethics & disclosures

Open Access fees and funding

Contact the journal

Submit manuscript

Working on a manuscript?

Avoid the most common mistakes and prepare your manuscript for journal editors.

Learn more →

Explore

Online first articles

Volumes and issues

Sign up for alerts

About this journal

Electronic ISSN 1572-834X

Print ISSN 0929-6212

Abstracted and indexed in

ACM Digital Library
BFI List
Baidu
CLOCKSS
CNKI
CNPIEC
Current Contents Collections / Electronics & Telecommunications Collection
DBLP
Dimensions
EBSCO Applied Science & Technology Source
EBSCO Associates Programs Source
EBSCO Computer Science Index
EBSCO Computers & Applied Sciences Complete
EBSCO Discovery Service
EBSCO Engineering Source
EBSCO Military Transition Support Center
EBSCO STM Source
EBSCO Science & Technology Collection
EBSCO Vocational Studies
EI Compendex
Google Scholar
INSPEC
Japanese Science and Technology Agency (JST)
Journal Citation Reports/Science Edition
Naver
OCLC WorldCat Discovery Service
Portico

ProQuest Advanced Technologies & Aerospace Database

ProQuest-ExLibris Primo

ProQuest-ExLibris Summon

SCImago

SCOPUS

Science Citation Index Expanded (SCIE)

TD Net Discovery Service

UGC-CARE List (India)

Wanfang

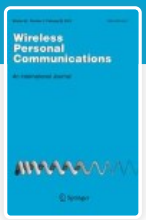

Wireless Personal Communications
An International Journal

Editors

Editor-in-Chief

Ramjee Prasad
ramjee@btech.au.dk
Professor, Future Technologies for Business Ecosystem Innovation (FT4BI),
President, CTIF Global Capsule (CGC)
Department of Business Development and Technology,
Aarhus University, Denmark

Associate Editors

Pardeep Kumar, QUEST University Nawabshah, Pakistan
Paulo P. Monteiro, University of Aveiro and Instituto de Telecomunicações, Portugal
Kashif Nisar, University Malaysia Sabah, Malaysia
Pablo Otero, University of Malaga, Malaga, Spain
Faisal K. Shaikh, Mehran University of Engineering & Technology, Jamshoro, Pakistan

Editorial Board

Matti Latva-aho
Director of 6G Flagship (www.6gflagship.com)
Centre for Wireless Communications
University of Oulu, Finland

Sumei Sun
Singapore Institute of Technology/Institute for Infocom Research
Singapore

Ma Maode
School of Electrical and Electronic Engineering at Nanyang Technological University

Geir Myrdahl Køien
USN, Campus Vestfold, Norway

Markus Eisenhauer
Luxembourg Institute of Science and Technology (LIST),
Esch-sur-Alzette, Luxembourg

May Huang
CGC, USA

Ashutosh Dutta
John Hopkins Applied Physics Laboratory, USA

Radosveta SOKULLU
Ege University, Turkey

Sanjay Kumar Biswash
NIIT University, India

For authors

Submission guidelines

Manuscript editing services

Ethics & disclosures

Open Access fees and funding

Contact the journal

Submit manuscript

Working on a manuscript?

Avoid the most common mistakes and prepare your manuscript for journal editors.

Learn more →

Explore

Online first articles

Volumes and issues

Sign up for alerts

Wireless Personal Communications
https://doi.org/10.1007/s11277-020-07754-9

Co-design Structure of Dual-Band LNA and Dual-Band BPF for Radio Navigation Aid Application

Gunawan Wibisono[1] · **Muh Wildan**[2] · **Johan Wahyudi**[2] · **Ego Widoro**[2] · **Teguh Firmansyah**[3]

Abstract

In this paper, a co-design of a dual-band low-noise amplifier (DB-LNA) with a dual-band band-pass filter (DB-BPF) for a radio navigation aid (RNA) application was proposed. The novel development was that the DB-LNA was directly integrated with the DB-BPF instead of connecting the output matching network (OMN) of the DB-LNA to the 50 Ω-port of the DB-BPF. Thus, this DB-BPF had a double function, serving as the DB-BPF and also as the OMN. This architecture was called the co-design structure. Z_{IN} analysis was used to evaluate the co-design network structure. In general, the design procedure was divided into four sections, including (1) DB-BPF, (2) DB-LNA, (3) Cascade DB-LNA and DB-BPF, and (4) Co-design DB-LNA and DB-BPF. The co-design method was applied in an RNA implementation at dual-band frequencies of 113 MHz and 332 MHz. Validation of the proposed structure is confirmed for its accuracy by simulating the impedance characteristic Z_{IN}, S parameter simulation, and measurement results. The key contributions of this paper were that: (1) The co-design structure could reduce the passive component by 31.5%, (2) the total size of the DB-LNA and DB-BPF using the co-design method was smaller than the cascaded method by 11.36%, (3) more light-weight in fabrication due to a smaller size, and (4) finally, the proposed LNA has a higher figure of merit than the other LNA.

✉ Gunawan Wibisono
gunawan@eng.ui.ac.id

Muh Wildan
m_wildan@yahoo.com

Johan Wahyudi
johanwahyudi99@yahoo.co.id

Ego Widoro
egoptpu@yahoo.com

Teguh Firmansyah
teguhfirmansyah@untirta.ac.id

[1] Department of Electrical Engineering, Faculty of Engineering, Universitas Indonesia, Kampus Baru UI Depok, Depok 16424, Indonesia

[2] Department of Aviation Engineering, Indonesian Civil Aviation Institute, Tangerang 15820, Banten, Indonesia

[3] Department of Electrical Engineering, Faculty of Engineering, Universitas Sultan Ageng Tirtayasa, Cilegon 42435, Banten, Indonesia

Published online: 29 August 2020

Keywords Co-design · Dual-band LNA · Dual-band BPF · VHF · Radio navigation aid

1 Introduction

In recent years, the radio wireless transceiver has had a great impact on modern society. The radio wireless transceiver includes important sub-systems, such as the antenna [1, 2] oscillator, mixer, power amplifier (PA), low noise amplifier (LNA) [3] and band-pass filter (BPF) [4]. For a single-band receiver, the design is relatively uncomplicated compared to the dual-band receiver architecture. Common receiver architectures include the heterodyne receiver, low intermediate frequency (IF) conversion, and direct conversion, where previous research has shown that their advantages and disadvantages [5, 6].

To improve the efficiency and support of the various types of communication equipment, a dual-band wireless transceiver terminal is required [7], as shown in Fig. 1. Moreover, a dual band wireless receiver consists of a dual-band antenna (DB-Antenna), dual-band oscillator (DB-Oscillator), dual-band mixer (DB-Mixer), dual-band LNA (DB-LNA), and dual-band BPF (DB-BPF). The DB-BPF and DB-LNA are important sub-systems of the dual-band receiver. There are several methods to produce the DB-BPF, such as the stepped impedance resonator (SIR) with short circuit terminated [8], parallel short-ended feed [9], net-type resonator [10], defected microstrip structure (DMS) [11], spiral resonator [12], self-feedback resonator [13], dual-transversal with multiple transmission zeros, combined SIR-defected ground structure (DGS) resonator, pseudo-interdigital SIR [14], dual E-shaped resonator [15], defected SIR and microstrip SIR [16], reconfigurable and tunable BPF, and low temperature co-fired ceramic (LTCC) technology [17]. However, the main problems in the DB-BPF filter method are that: (1) It is difficult to manufacture/fabricate, (2) requires heat removal, (3) has unwanted coupling, (4) has a parasitic effect, (5) has a complex structure, (6) requires active components and power supply, (7) has high harmonics, (8) involves filter package problems, and (9) it has a mono-function/stand-alone function (only as a DB-BPF).

Similar to the DB-BPF design method, methods to produce the DB-LNA include the wideband LNA by transformer [18], wideband LNA employing a cascaded complimentary [19], and an inductorless wideband LNA [20]. Wideband LNA has several advantages, such as low power, high immunity to multipath fading, and potentially high data rates. Furthermore, References [21, 22] proposed a reconfigurable LNA. However, the main problem in a reconfigurable LNA is that it requires good switching technology performance. This switch is commonly based on varactors, mechanical actuators, tunable materials,

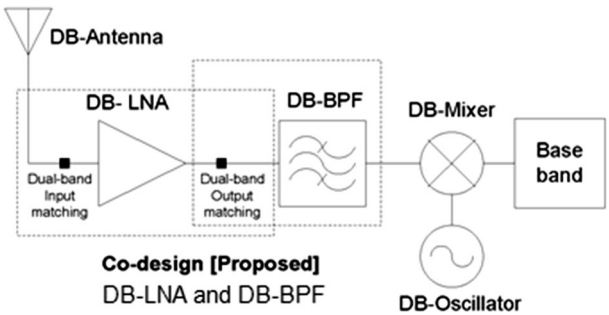

Fig. 1 The proposed co-design structure of DB-BPF as the output matching of DB-LNA in the dual band wireless receiver

microelectro-mechanicals (MEMS), and radio frequency (RF) switches. Moreover, References [23] proposed a concurrent LNA, where the concurrent method successfully created a dual-band/multi-band matching networks structure. This method has advantages such as good power efficiency, less passive components, low interferences, low noise, and high gains at two or more frequencies simultaneously. In the conventional dual-band receiver architecture, the DB-BPF is directly connected to the output port (IMN)/output matching networks (OMN) of the DB-LNA to achieve good frequency selectivity. Therefore, the DB-LNA and DB-BPF must be designed separately, which requires a lot of passive components and results in large dimensions. Both the DB-BPF and DB-LNA have a mono-/stand-alone function, respectively.

The co-design method has attracted the attention of many researchers, because this method enables a sub-system with multi-functions. For instance, Wu et al. introduced a co-design dual-band filter-antenna [24]. Instead of using the traditional 50 Ω, their research proposed a dual-band monopole antenna with a dual-band pseudo-interdigital bandpass as matching networks. The results showed that the filter-antenna achieved a good filter and antenna performance. Zhang et al. [25] combined filters and an oscillator to reduce the second and third harmonics. As a result, the co-design filters and oscillator significantly improved the quality of the signal and phase noise. Furthermore, References [26, 27] investigated the co-design of the DB LNA and the BPF. The BPF was used at both the IMN and the OMN. However, the circuit size was still large because the component reduction was not significant.

In this paper, a co-design structure of the DB-LNA and DB-BPF as the OMN for a dual-band radio navigation aid (RNA) application is proposed, as shown in Fig. 1. Our novel development is that, in order to reduce the passive components, a co-design method is used by directly integrating the DB-LNA and DB-BPF without DB OMNs. Consequently, this DB-BPF has a double function, serving as the DB-BPF and as an OMN. To verify the co-design method, the DB-LNA and DB-BPF were simulated, fabricated, and measured accordingly. We used a center frequency at 113 MHz and 332 MHz, respectively, and a transistor 2N3583 with a DC Bias of $V_{CC}=12$ V, $V_{CE}=2$ V, $I_C=10$ mA, and $\beta=110$ was used, whilst the degenerative structure with $L_E=1$ nH and $C_{BE}=3.9$ pF was applied to the DC bias structure.

The design method was divided into four model as shown in Fig. 2, including the: (a) DB-BPF, (b) DB-LNA, (c) cascade DB-LNA and DB-BPF, and (d) co-design DB-LNA and DB-BPF. The procedure followed in this paper could be detailed as follows. First, the DB-BPF was designed based on a lumped component, and the lower- and upper-band analysis were used to investigate the resonator circuit. Second, the DB-LNA with dual-band input/output matching circuit was constructed, and the matching circuit networks were designed under the principle of impedance conjugated matching. Third,

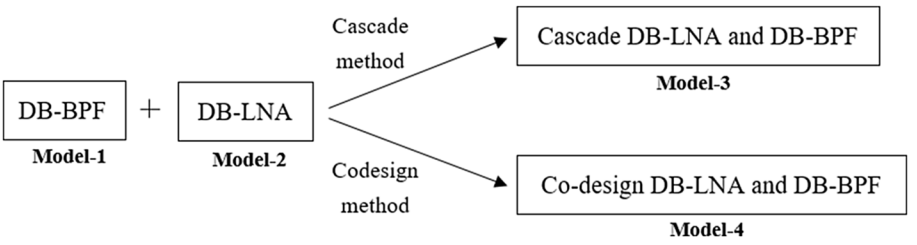

Fig. 2 Proposed model of circuit design

the DB-LNA was cascaded with the DB-BPF, which is a commonly used conventional method. Fourth, the co-design of the DB-LNA and DB-BPF was applied, where the output port of the DB-LNA was directly connected/cascaded to the input port of the DB-BFP, without the output matching networks of the DB-LNA. Therefore, the DB-BPF had a dual function, serving not only as a filter but also as an OMN circuit. Simulation and optimization of the proposed methods was performed using the Advance Design System (ADS) software.

2 Design Methods

2.1 DB-BPF [Model-1]

The first section involved the design of the BD-BPF based on a lumped element, as shown in Fig. 3. This lumped element was based on the Butterworth filter model, refer to the design in Ref. [28]. The components C_{A1}, C_{A4}, and C_{A5} are the coupling capacitor, and L_{A1} is the coupling inductor. Furthermore, the upper-line indicates the lower-band circuit and the lower-line shows the upper-band circuit.

The first step of the DB-BPF design was to set the lower passband frequency (ω_{LB}). The component value for the element at the lower passband frequency was defined by the resonators L_{A2} and C_{A2} or L_{A3} and C_{A3} at the related frequency resonance were given by [28]:

$$\omega_{LB} = \frac{1}{\sqrt[2]{L_{A2}C_{A2}}} = \frac{1}{\sqrt[2]{L_{A3}C_{A3}}} \tag{1}$$

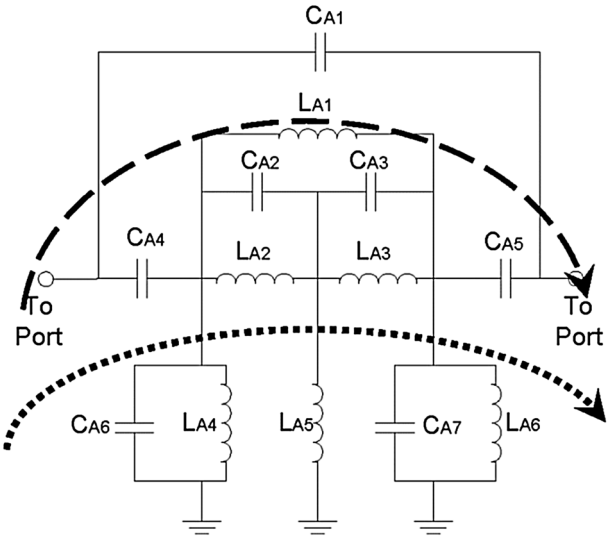

Fig. 3 DB-BPF based a on lumped element, as in Ref [28]

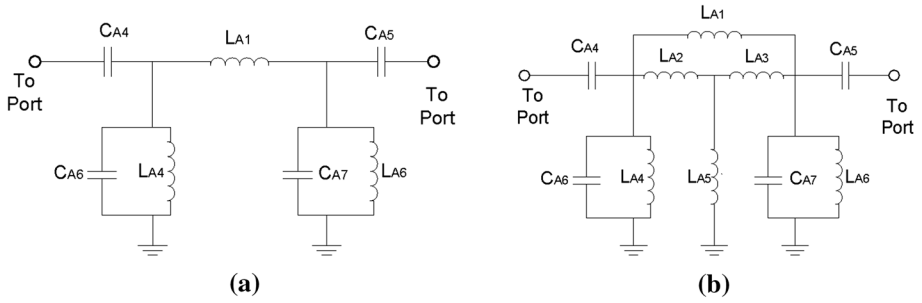

Fig. 4 **a** Lower-band and **b** Upper-band of the DB-BPF schematic, as described in Ref. [28]

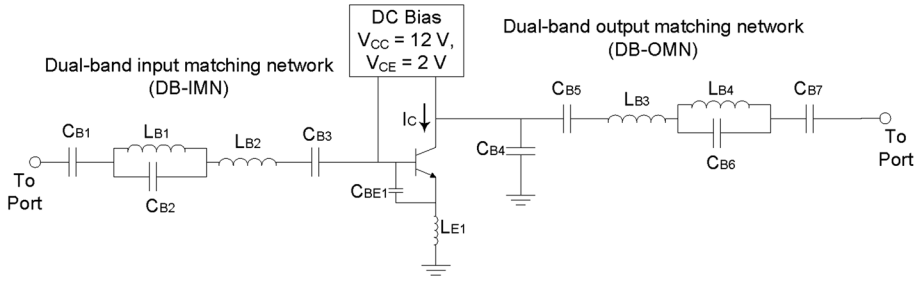

Fig. 5 The proposed DB-LNA with a DB-IMN and DB-OMN

where the value of $L_{A2}=L_{A3}$ and $C_{A2}=C_{A3}$, and ω_C is the resonant frequency. The second band could be tuned by the parametric iteration of L_{A6} and C_{A4} or L_{A6} and C_{A7}, and the center frequency of the upper band resonant (ω_{UB}) were given by [28];

$$\omega_{UB}=\frac{1}{\sqrt[2]{C_{A6}+\frac{C_{A4}}{1+\left(\omega_{LB}Z_oC_{A4}\right)^2\left(\frac{L_{A4}\left(2L_{A5}-0.27L_{A2}\right)}{L_{A4}+2L_{A5}-0.27L_{A2}}\right)}}} \tag{2}$$

The upper-band resonant (ω_{UB}) could be adjusted without affecting the lower band. Therefore, the lower-band and upper-band schematics are shown in Fig. 4a, b, respectively.

Figure 4a illustrates that the coupling inductor at the lower-band circuit was generated by L_{A1}. The upper-band shown in Fig. 4b, the L_{A1} served not only as a coupling, but it also produced the second-band by cooperating with L_{A2}, L_{A3}, and L_{A5}.

2.2 DB-LNA [Model-2]

As proposed, the second section provides a brief on the DB-LNA design. The proposed DB-LNA was constructed using the direct current (DC) bias structure and a DB IMN/OMN, as shown in Fig. 5. In this study, a transistor 2N3583 with a DC Bias of $V_{CC}=12$ V, $V_{CE}=2$ V, and $I_C=10$ mA was used, it also added components of the radio frequency choke (RFC) for blocking the DC. The DB-LNA had an emitter degenerative structure with $L_{E1}=1$ nH and $C_{BE1}=3.9$ pF, as shown in Fig. 5.

The inductor (L_{E1}) and capacitor (C_{BE1}) have function to reduce the noise value and maintain stability of the circuit at a value of $K>1$. Furthermore, this DB-LNA had a

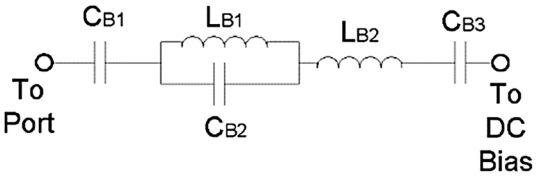

Fig. 6 The output port IMN of the DB-LNA

DB IMN as shown in Fig. 6. The DB IMN with the specific circuit included a $L_{B2}C_{B3}$ series resonating circuit cascaded with a $L_{B1}C_{B2}$ shunt resonating as depicted in Fig. 6. This DB IMN was constructed under the principle of impedance conjugated matching.

The matching circuit networks could resonate at two different frequencies simultaneously. This condition could be shown by plotting the impedance characteristics of the LC shunt of L_{B1} and C_{B2}, as shown in Fig. 7.

Figure 7 shows the impedance characteristics of the imaginary-part of the $L_{B1}C_{B2}$ shunt. For the $L_{B1}C_{B2}$ shunt at the IMN at a low frequency of 113 MHz, its impedance becomes more inductive, thus it is equivalent to an inductance L_A as shown in Fig. 8a. Then, at a high frequency of 332 MHz, its impedance circuit appears capacitive, so it is equivalent to a capacitance C_A as shown in Fig. 8b. Furthermore, the Eqs. (2) and (3) can determine the frequency resonant.

Based on Fig. 8a, b, IMNs could resonate at two frequencies of $f_1 = 113$ MHz and $f_2 = 332$ MHz when the component values of C_{B1}, L_{B2}, C_{B3}, L_A, and C_A are properly chosen according to the following equations

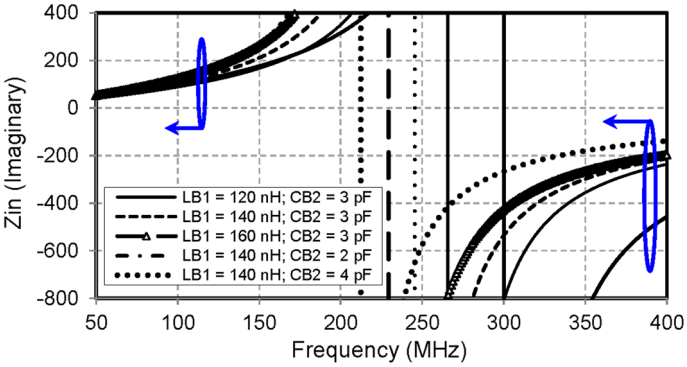

Fig. 7 Z_{IN} impedance characteristics of the imaginary-part of the LC shunt of L_{B1} and C_{B2}

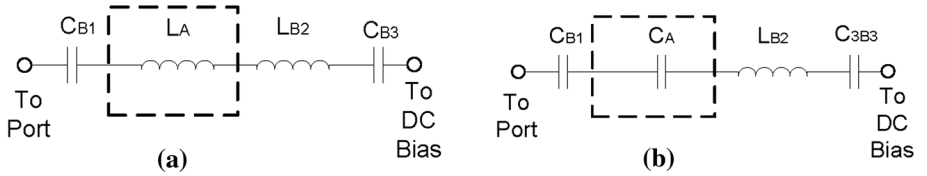

Fig. 8 **a** Equivalent circuit of the IMN of the DB-LNA at the resonant condition at 113 MHz, **b** 332 MHz

$$f_1 = \frac{1}{2\pi}\sqrt{\frac{C_{B1}+C_{B3}}{(L_{B2}+C_A)(C_{B1}C_{B3})}} \tag{3}$$

$$f_2 = \frac{1}{2\pi}\sqrt{\frac{C_AC_{B3}+C_{B1}C_{B3}+C_{B1}C_A}{L_{B2}(C_{B1}C_AC_{B3})}} \tag{4}$$

The small signal equivalent circuit of the DB-LNA and the IMN circuit are shown in Fig. 9. At the small signal analysis, the transistor consists of g_1, C_{BE1}, and L_{E1} as the transconductance, coupling capacitor, and degenerative structure, respectively. Meanwhile the DB-IMN consists of C_{BE1}, C_{BE2}, C_{BE3}, L_{B1}, and L_{B1}.

An input impedance Z_{IN} is given by

$$Z_{IN} = \frac{1}{j\omega C_{B1}} + \frac{1-\omega^2 C_{B2}L_{B1}}{j\omega L_{B1}} + j\omega L_{B2} + \frac{1}{j\omega C_{B3}} + \frac{L_E}{C_{BE1}}g_{m1} \tag{5}$$

At the matching condition, the conjugate complex source impedance (Z_S*) must equal the load impedance (Z_{IN}), so that maximum power transfer can be obtained. The matching Z_{IN} and S_{11} are given by:

$$Z_{IN} = Z_S^* = \frac{L_{E1}}{C_{BE1}}g_{m1} = 50\Omega \tag{6}$$

$$S_{11} = \frac{Z_{IN}-Z_S}{Z_{IN}+Z_S} \tag{7}$$

$$\begin{aligned} S_{11} &= \frac{\left(\frac{1}{j\omega C_{B1}} + \frac{1-\omega^2 C_{B2}L_{B1}}{j\omega L_{B1}} + j\omega L_{B2} + \frac{1}{j\omega C_{B3}} + \frac{L_{E1}}{C_{BE1}}g_{m1}\right) - \left(\frac{L_{E1}}{C_{BE1}}g_{m1}\right)}{\left(\frac{1}{j\omega C_1} + \frac{1-\omega^2 C_2 L_1}{j\omega L_1} + j\omega L_2 + \frac{1}{j\omega C_3} + \frac{L_E}{C_{BE}}g_m\right) + \left(\frac{L_E}{C_{BE}}g_m\right)} \\ &= \frac{\frac{1}{j\omega C_{B1}} + \frac{1-\omega^2 C_{B2}L_{B1}}{j\omega L_{B1}} + j\omega L_{B2} + \frac{1}{j\omega C_{B3}}}{\frac{1}{j\omega C_{B1}} + \frac{1-\omega^2 C_{B2}L_{B1}}{j\omega L_{B1}} + j\omega L_{B2} + \frac{1}{j\omega C_{B3}} + 2\frac{L_{E1}}{C_{BE1}}g_{m1}} \end{aligned} \tag{8}$$

With $j\omega = s$ at resonant frequency (ω_0), the Eq. (8) could be simplified as

$$S_{11} = \frac{As^2 - \omega B + C + D + E}{As^2 + 100sF - \omega B + C + D + E} \tag{9}$$

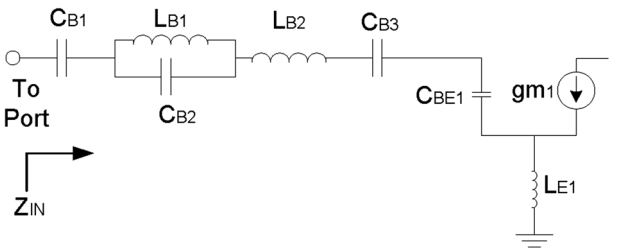

Fig. 9 The small signal equivalent circuit and the DB-IMN of the DB-LNA

where

$$\begin{aligned} A &= L_{B1}L_{B2}C_{B1}C_{B3} \\ B &= L_{B1}C_{B1}C_{B2}C_{B3} \\ C &= L_{B1}C_{B3} \\ D &= C_{B1}L_{B1} \\ E &= C_{B1}C_{B3} \end{aligned} \tag{10}$$

the stability factor (K) of this DB-LNA is given by [27]:

$$K = \frac{\left(1 + \left|S_{11}S_{22} - S_{12}S_{21}\right|^2 - \left|S_{11}\right|^2 - \left|S_{22}\right|^2\right)}{\left(2 * \left|S_{12}S_{21}\right|\right)} \tag{11}$$

where S_{21} is the gain and S_{22} is the output reflection coefficient.

2.3 Cascade Structure DB-LNA and DB-BPF [Model-3]

This section discusses a cascaded structure of the DB-LNA and DB-BPF as illustrated in Fig. 10. A cascaded structure of the DB-LNA and DB-BPF was constructed using the dual-band IMN/OMN, DC bias, and DB-BPF. The dual-band OMN was directly connected/cascaded to the input port of the DB-BFP.

2.4 Co-design Structure of the DB-LNA and DB-BPF [Model-4]

This section discusses the co-design structure of the DB-LNA and DB-BPF. The DB-LNA was directly integrated with the DB-BPF, instead of connecting the OMN to the 50 Ω-port of the DB-BPF. Therefore, this DB-BPF had a double function, working not only as the DB-BPF but also as the OMN. In this study, Z_{IN} analysis was used to evaluate the co-design network structure. The process details of the co-design methods are described as follows:

(1) Draw the full circuit of the DB-OMN and DB-BPF, and then separate them into the lower-band and upper band parts, such as the lower-band OMN, lower-band DB-BPF,

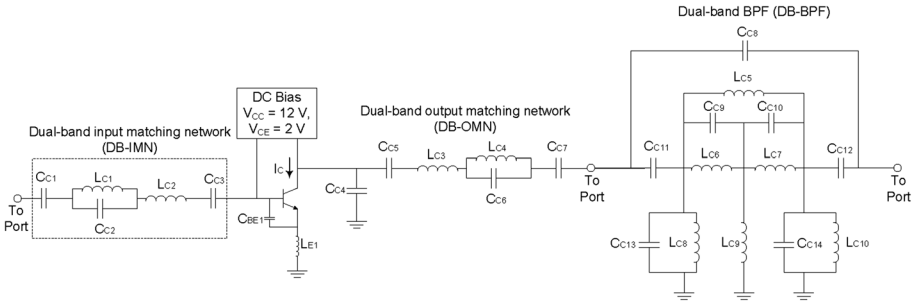

Fig. 10 The proposed cascade structure of the DB-LNA and DB-BPF

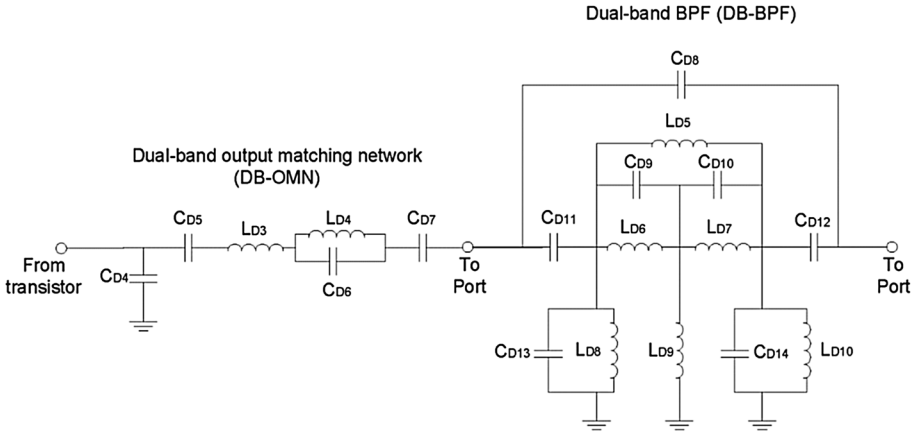

Fig. 11 The full circuit of the DB-OMN and DB-BPF

upper-band OMN, and upper-band DB-BPF. Figure 11 illustrates the full circuit of the DB-OMN and DB-BPF.

(2) Determine the impedance characteristic at the lower-band and upper-band conditions, as shown in Fig. 12a. In particular, Fig. 12a shows the impedance characteristic of the imaginary-part of the $L_{D4}C_{D6}$ shunt of the DB-OMN. At the low frequency of

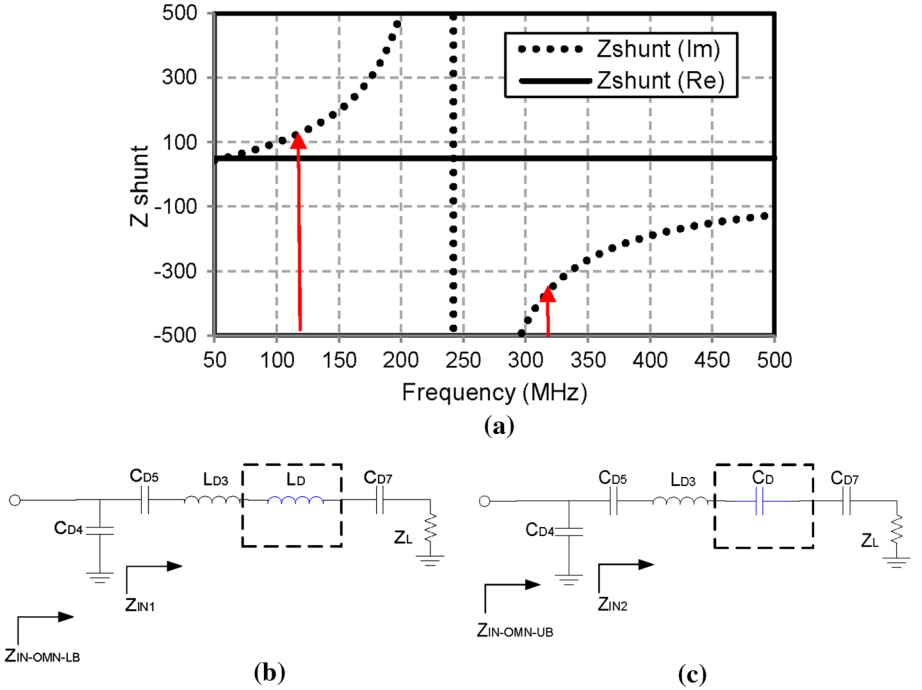

Fig. 12 **a** The impedance characteristic of the imaginary-part of the $L_{D4}C_{D6}$ shunt of the DB-OMN, **b** Equivalent DB-OMN circuit at the lower band, **c** Equivalent DB-OMN circuit at the upper band

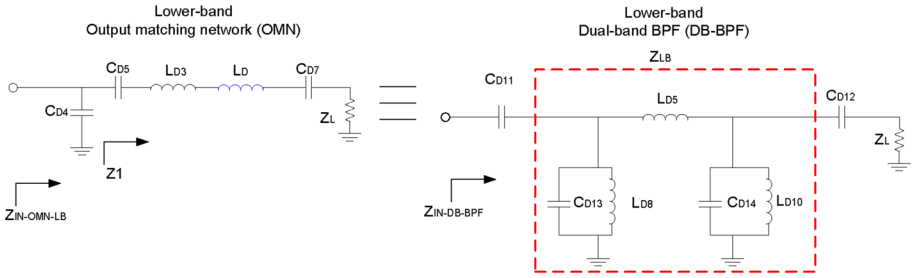

Fig. 13 The circuit of the OMN and DB-BPF at the lower-band resonant condition

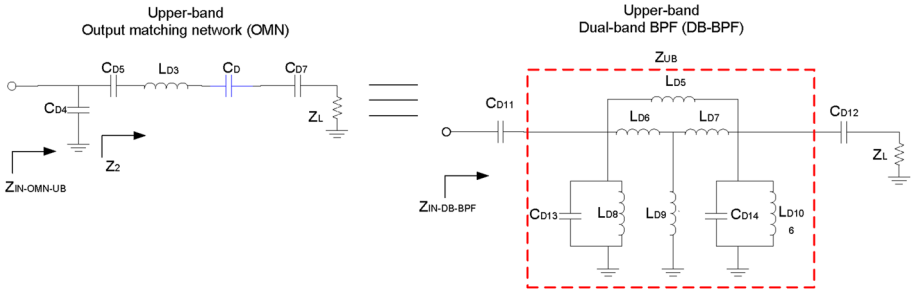

Fig. 14 The circuit of the OMN and DB-BPF at the upper-band resonant condition

113 MHz, its impedance becomes more inductive with positive imaginary impedance, so it is equivalent to the inductance L_D as shown in Fig. 12b. Then, at a high frequency of 332 MHz, its impedance circuit appears capacitive with negative imaginary impedance, so it is equivalent to the capacitance C_D as shown in Fig. 12c.

(3) At the resonant condition, to ensure that the co-design is operating, the value of the $Z_{IN\text{-}OMN}$ must be equal to the $Z_{IN\text{-}DB\text{-}BPF}$ value, at both the lower-band and upper-band simultaneously, as shown in Figs. 13 and 14. The $Z_{IN\text{-}OMN\text{-}LB}$, $Z_{IN\text{-}OMN\text{-}UB}$, $Z_{IN\text{-}DB\text{-}BFB}$ refer to the Z_{IN} of the OMN at the lower band, Z_{IN} of the OMN at the upper-band, and Z_{IN} of the DB-BPF, respectively.

As shown in Fig. 13, at the low-band resonant condition, the Z_{IN} of the OMN at the lower band ($Z_{IN\text{-}OMN\text{-}LB}$) network is given by:

$$Z_1 = \frac{1}{j\omega C_{D5}} + j\omega L_{D3} + j\omega L_D + \frac{1}{j\omega C_{D7}} + Z_L \tag{12}$$

$$\begin{aligned} Z_{IN-OMN-LB} &= \left(\frac{1}{Z_1} + j\omega C_{D4}\right)^{-1} \\ &= \frac{C_{D7} - \omega^2 L_{D3} C_{D5} C_{D7} + C_{D5} + j\omega C_{D5} C_{D7} Z_L}{j\omega C_{D4}\left(C_{D7} - \omega^2 L_{D3} C_{D5} C_{D7} + C_{D5} + j\omega C_{D5} C_{D7} Z_L\right) + j\omega C_{D5} C_{D7}} \end{aligned} \tag{13}$$

Moreover, at the low-band resonant condition, the value of $Z_{IN\text{-}OMN\text{-}LB}$ must be equal to the $Z_{IN\text{-}DB\text{-}BPF}$ value. In other words, the resonator (Z_{LB}) can be given by:

$$Z_{LB} = \frac{C_{D7} - \omega^2 L_{D3} C_{D5} C_{D7} + C_{D5} + j\omega C_{D5} C_{D7} Z_L}{j\omega C_{D4}\left(C_{D7} - \omega^2 L_{D3} C_{D5} C_{D7} + C_{D5} + j\omega C_{D5} C_{D7} Z_L\right) + j\omega C_{D5} C_{D7}} - \frac{C_{D12} + C_{D11} + j\omega C_{D11} C_{D12} Z_L}{j\omega C_{D11} C_{D12}} \tag{14}$$

The value of the impedance characteristic of the $L_{D4}C_{D6}$ shunt of the DB-OMN at a frequency of 332 MHz is more capacitive, so it is equivalent to the capacitance C_D. The impedance Z_2 is given by:

$$Z_2 = \frac{1}{j\omega C_{D5}} + j\omega L_{D3} + \frac{1}{j\omega C_{D5}} + \frac{1}{j\omega C_{D7}} + Z_L \tag{15}$$

As shown in Fig. 14, at the upper-band resonant condition, the Z_{IN} of the OMN at the upper-band ($Z_{IN\text{-}OMN\text{-}UB}$) network is given by:

$$\begin{aligned} Z_{IN-OMN-UB} &= \left(\frac{1}{Z_{IN2}} + j\omega C_{D4}\right)^{-1} \\ &= \frac{C_D C_{D7} - \omega^2 L_{D3} C_{D5} C_D C_{D7} + C_{D5} C_{D5} + j\omega C_{D5} C_{D7} Z_L}{j\omega C_{D4}\left(C_D C_{D7} - \omega^2 L_{D3} C_{D5} C_D C_{D7} + C_{D5} C_{D5} + j\omega C_{D5} C_{D7} Z_L\right) + j\omega C_{D5} C_D C_{D7}} \end{aligned} \tag{16}$$

Moreover, at the upper-band resonant condition, the value of $Z_{IN\text{-}OMN\text{-}UB}$ must be equal to the $Z_{IN\text{-}DB\text{-}BPF}$ value. In other words, the resonator (Z_{UB}) can be given by

$$Z_{UB} = \frac{C_D C_{D7} - \omega^2 L_{D3} C_{D5} C_D C_{D7} + C_{D5} C_{D5} + j\omega C_{D5} C_{D7} Z_L}{j\omega C_{D4}\left(C_D C_{D7} - \omega^2 L_{D3} C_{D5} C_D C_{D7} + C_{D5} C_{D5} + j\omega C_{D5} C_{D7} Z_L\right) + j\omega C_{D5} C_D C_{D7}} - \frac{C_{D12} + C_{D11} + j\omega C_{D11} C_{D12} Z_L}{j\omega C_{D11} C_{D12}} \tag{17}$$

(4) To verify the co-design method, Fig. 15a–d show the comparisons of the simulation results of the impedance characteristic, split according to the real and imaginary-part of the DB-OMN and DB-BPF at the lower-band frequency of 113 MHz and the upper-band frequency of 332 MHz. The results showed that the values of the impedance characteristic were equal at the resonance frequencies.
(5) Moreover, Fig. 16a, b exhibit the comparisons of the input reflection coefficient (S_{11}) of the DB-OMN and DB-BPF. These findings also supported the condition that the DB-BPF has a double function, working not only as the DB-BPF but also as the OMN.
(6) Finally, Fig. 17 presents a circuit with the co-design structure of the DB-LNA and DB-BPF.

To compare the DB-LNA design method, the calculation of figure of merit (FoM) is used, where FoM is given by;

$$FoM\left[mW^{-1}\right] = \frac{Gain[abs]}{(NF-1)[abs] \cdot P_{DC}[mW]} \tag{18}$$

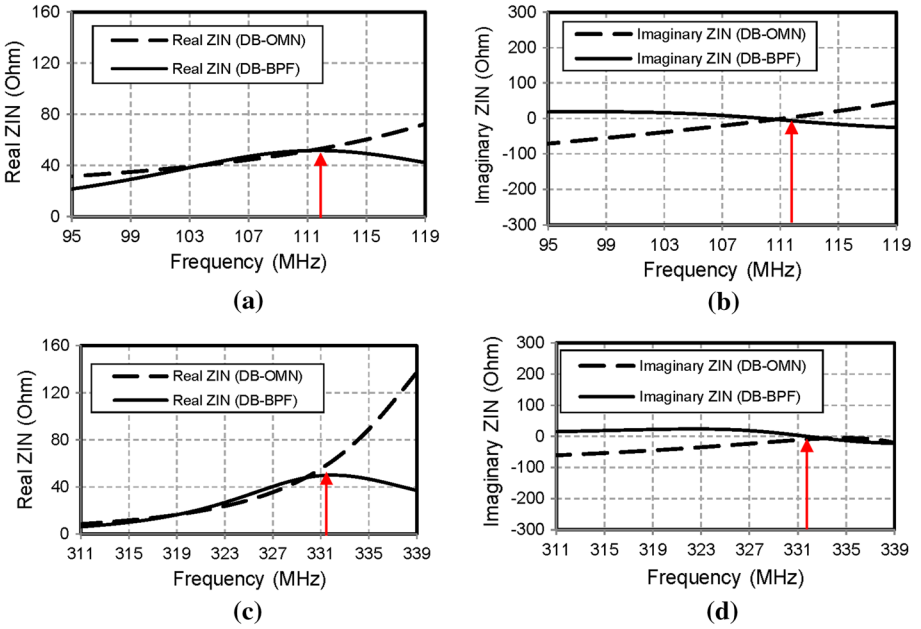

Fig. 15 The comparison of the impedance characteristic between the DB-OMN and DB-BPF, **a** Real-part at a frequency of 113 MHz, **b** Imaginary-part at a frequency of 113 MHz, **c** Real-part at a frequency of 332 MHz, **d** Imaginary-part at a frequency of 332 MHz

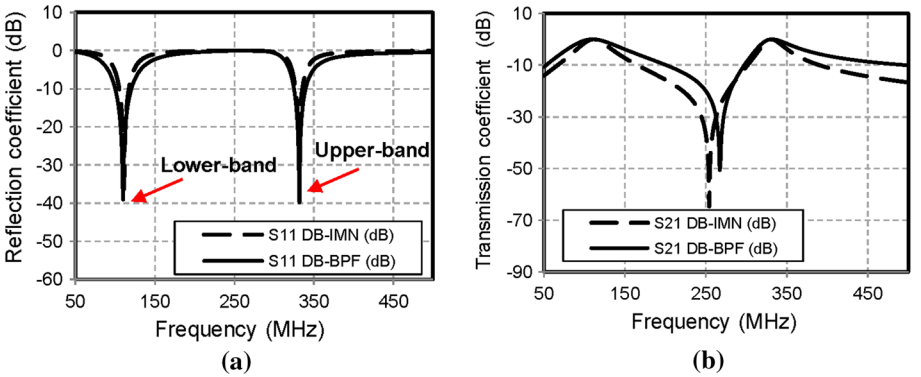

Fig. 16 The comparison of **a** S_{11} (dB) and **b** S_{21} (dB) of the DB-OMN and DB-BPF

3 Design Implementation

In this section, DB-BPF and DB-BPF for RNA application at a dual-band frequency of 113 MHz and 332 MHz was simulated, fabricated, and measured. The implementation of this design was divided into four parts including: (1) DB-BPF, (2) DB-LNA, (3) Cascade DB-LNA and DB-BPF, and (4) Co-design DB-LNA and DB-BPF.

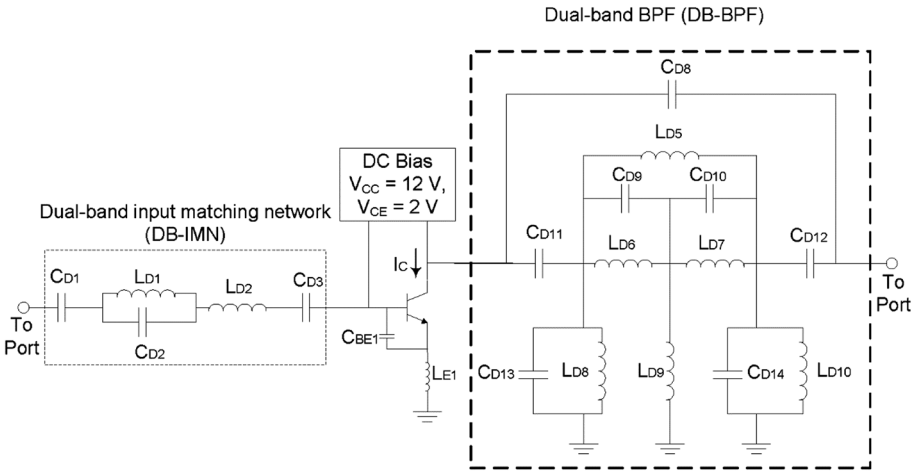

Fig. 17 Co-design structure of the DB-LNA and DB-BPF

3.1 DB-BPF [Model-1]

Figure 3 illustrates the final DB-BPF based on the lumped element. The numerical iteration and the dependency of S_{21} and S_{11} on the varied L_{A4} and C_{A3} are given clearly in Fig. 18a, b. The figures show that by increasing L_{A4} and C_{A3}, the lower center frequencies would be stable. However, increasing the L_{A4} and C_{A3} would slightly raise the fractional bandwidth (FBW). Furthermore, the variation of L_4 and C_3 would change the transmission zeros (T_Z) of this filter.

After optimization of the filter structure, the value of the circuit became $L_{A1}=0.5$ nH, $L_{A2}=L_{A3}=19.45$ nH, $L_{A4}=L_{A6}=68$ nH, $L_{A5}=11.85$ nH, $C_{A1}=20$ pF, $C_{A2}=C_{A3}=19.45$ pF, $C_{A4}=C_{A5}=200$ pF, and $C_{A6}=C_{A7}=26.2$ pF. The final result of the DB-BPF response is shown in Fig. 19.

Figure 19 shows the value of the S_{21} (dB) and S_{11} (dB) of the DB-BPF. Moreover, the bandwidth (BW) of the DB-BPF was given at the value of S_{21} (dB) $=-3$ dB. At the

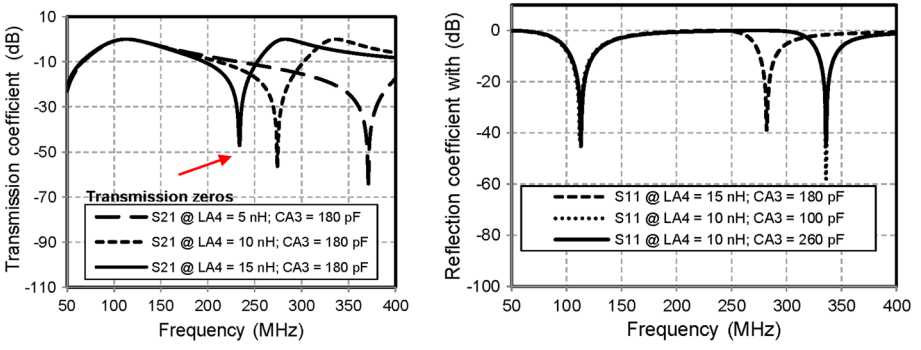

Fig. 18 The simulation of **a** S_{21} (dB) and **b** S_{11} (dB) with varied L_{A4} and C_{A3}

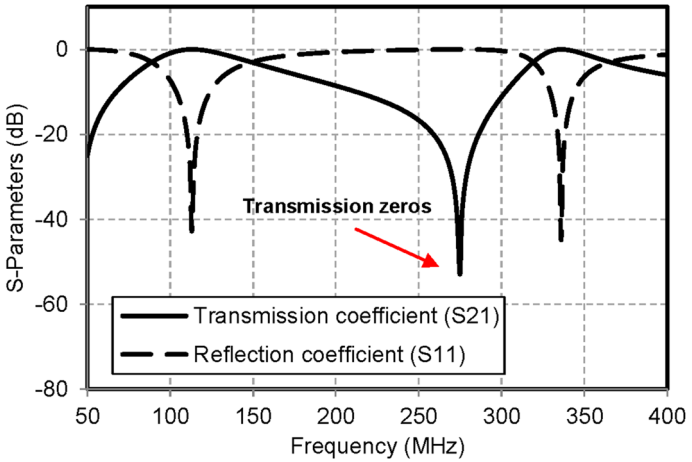

Fig. 19 The value of the S_{21} (dB) and S_{11} (dB) response of the DB-BPF

lower-band with a frequency center of 113 MHz, the DB-BPF was $S_{21} = -0.336$ dB, $S_{11} = -42.78$ dB, and BW = 61 MHz. Furthermore, at the upper-band, with a frequency center of 332 MHz, the DB-BPF was $S_{21} = -0.265$ dB, $S_{11} = -44.85$ dB, and BW = 47 MHz. Furthermore, the transmission zeros (T_Z) of the DB-BPF was −52.28 dB at 275 MHz.

3.2 DB-LNA [Model-2]

Figure 5 shows the proposed DB-LNA. The dependency of the S_{11} response on the varied L_{B1} and C_{B2} is shown in Fig. 20. The figure shows that by increasing the L_{B1}, the low center frequency was still stable, but at an upper frequency, this changed significantly. It

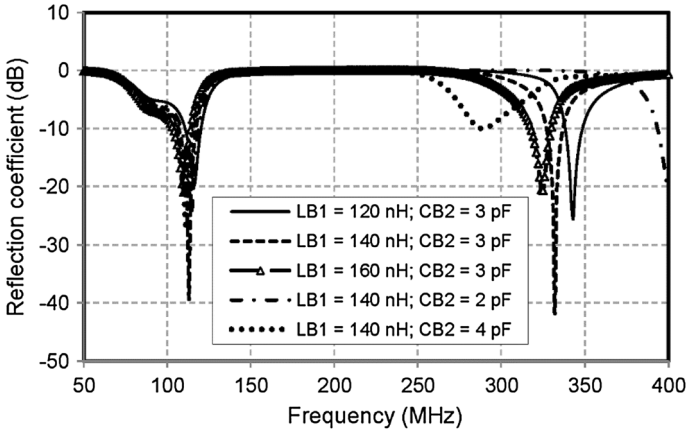

Fig. 20 S_{11} response with varied L_{B1} and C_{B2}

also showed that at $L_{B1}=140$ nH and $C_{B2}=4$ pF, the upper frequency was resonated at 400 MHz.

After optimization of the DB-LNA, the value of the circuit became $L_{B1}=140$ nH, $L_{B2}=220$ nH, $L_{B3}=250$ nH, $L_{B4}=130$ nH, $C_{B1}=130$ pF, $C_{B2}=3$ pF, $C_{B3}=6$ pF, $C_{B4}=5$ pF, $C_{B5}=6$ pF, $C_{B6}=3$ pF, and $C_{B7}=100$ pF. The transistor 2N3583 with a DC Bias of $V_{CC}=12$ V, $V_{CE}=2$ V, $I_C=10$ mA, and $\beta=110$ was used, with $L_{E1}=1$ nH and $C_{BE1}=3.9$ pF. The performance of the DB LNA characterized by S_{11} (dB), gain S_{21} (dB), noise figure (nf), and the stability factor (K) is shown in Fig. 20. Figure 20 shows that the results of the DB-LNA characterized by S_{11}, S_{21}, nf, K were −39.3 dB, 24.11 dB, 1.28 dB, 1.15, respectively, at 113 MHz, and −41.84 dB, 18.19 dB, 1.25 dB, 1.17, respectively, at 332 MHz. Figure 21 also shows that the minimum value of nf and S_{11} appears at the resonance frequency. Furthermore, the value of K had an increasing trend. This data indicated that the DB-LNA had very good stability performance.

3.3 Cascade Structure DB-LNA and DB-BPF [Model-3]

This section discusses the cascade structure of the DB-LNA and DB-BPF as illustrated in Fig. 10. A cascade structure of the DB-LNA and DB-BPF was constructed using the dual-band IMN/OMN, DC bias, and DB-LNA. The DB-OMN was directly connected/cascaded to the input port of the DB-BFP. After the numerical optimization of the DB-LNA, the values of the circuit became $L_{C1}=140$ nH, $L_{C2}=220$ nH, $L_{C3}=250$ nH, $L_{C4}=130$ nH, $L_{C5}=0.5$ nH, $L_{C6}=L_{C7}=19.45$ nH, $L_{C8}=L_{C10}=68$ nH, $L_{C9}=11.85$ nH, $C_{C1}=130$ pF, $C_{C2}=3$ pF, $C_{C3}=6$ pF, $C_{C4}=5$ pF, $C_{C5}=6$ pF, $C_{C6}=3$ pF, $C_{C7}=100$ pF, $C_{C8}=20$ pF, $C_{C9}=C_{C10}=19.45$ pF, $C_{C11}=C_{C12}=200$ pF, and $C_{C13}=C_{C14}=26.2$ pF. The transistor 2N3583 with a DC Bias of $V_{CC}=12$ V, $V_{CE}=2$ V, $I_C=10$ mA, and $\beta=110$ was used, with $L_{E1}=1$ nH and $C_{BE1}=3.9$ pF.

Given that both the output port of the DB-LNA and the input port of the DB-BPF had impedance of 50 Ω, the port could be directly connected. The performance of the cascaded DB-LNA and DB-BPF was characterized by S_{11} (dB), S_{21} (dB), nf, and K, are shown in Fig. 22. The results of the DB-LNA shown by S_{11}, S_{21}, nf, K were −39.3 dB, 24.11 dB,

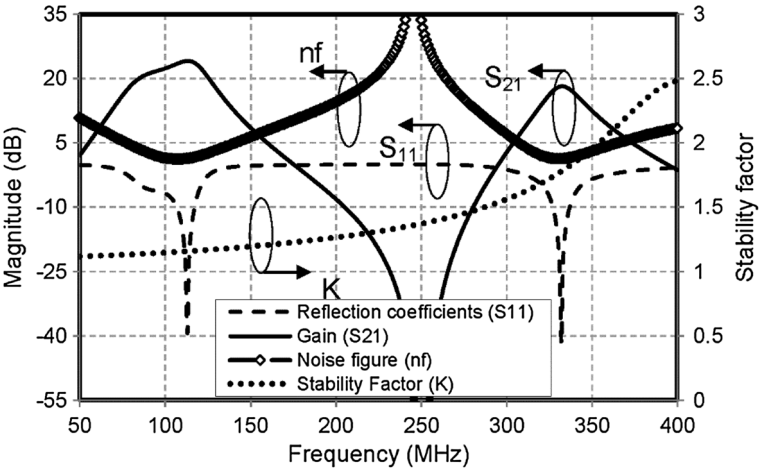

Fig. 21 The simulation results of the S_{11} (dB), gain S_{21} (dB), nf, and K of the DB-LNA

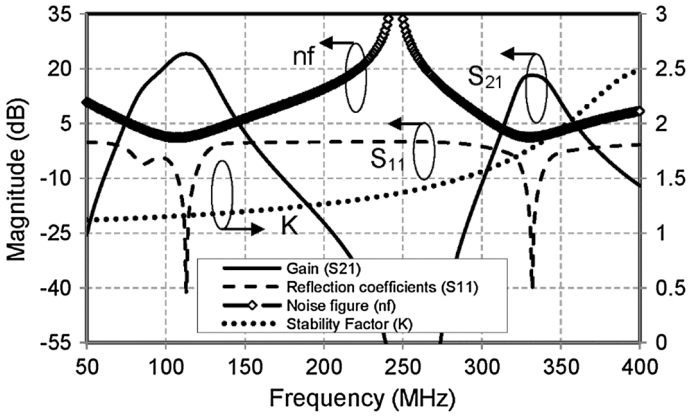

Fig. 22 The simulation result of the S_{11} (dB), gain S_{21} (dB), nf, and K of the cascade structure DB-LNA and DB-BPF

1.28 dB, 1.14, respectively, at 113 MHz, and −41.84 dB, 18.11 dB, 1.25 dB, 1.36, respectively, at 332 MHz. Figure 22 also shows that the minimum value of the nf and S_{11} were at the resonance frequency. Furthermore, the value of K had an increasing trend. This indicated that the LNA had good stability.

3.4 Co-design Structure DB-LNA and DB-BPF [Model-4]

The co-design structure of the DB-LNA and DB-BPF is shown in Fig. 17. The DB-BPF had a double function, serving not only as the DB-BPF but also as the OMN. After the numerical iteration of the co-design structure of the DB-LNA and DB-BPF, the values of the circuit became $L_{D1}=140$ nH, $L_{D2}=220$ nH, $L_{D5}=0.5$ nH, $L_{D6}=L_{D7}=19.45$ nH, $L_{D8}=L_{D10}=68$ nH, $L_{D9}=11.85$ nH, $C_{D1}=130$ pF, $C_{D2}=3$ pF, $C_{D3}=6$ pF, $C_{D8}=20$ pF, $C_{D9}=C_{D10}=19.45$ pF, $C_{D11}=C_{D12}=200$ pF, and $C_{D13}=C_{D14}=26.2$ pF. The transistor 2N3583 with a DC Bias of $V_{CC}=12$ V, $V_{CE}=2$ V, $I_C=10$ mA, and $\beta=110$ was used, with $L_{E1}=1$ nH and $C_{BE1}=3.9$ pF. The results of the co-design DB-LNA and DB-BPF are shown in Fig. 23.

The results of the DB-LNA shown by S_{11}, S_{21}, nf, K were −25.12 dB, 24.11 dB, 1.28 dB, 1.15, respectively, at 113 MHz, and −30.22 dB, 17.21 dB, 1.25 dB, 1.17, respectively, at 332 MHz. Figure 22 also shows that the minimum value of nf and S_{11} was at the resonance frequency. Furthermore, the value of K had an increasing trend. The high stability factor indicated that the LNA would be stable working at higher frequencies and would not oscillate.

4 Result and Discussion

To validate the design, the proposed circuit was fabricated on a printed circuit board (PCB) with a double-layer FR4 substrate, with a constant dielectric (ε_r) that was 4.3 and 1.6 mm thick. The type of transmission line used was grounded with a coplanar structure. Figure 24 shows the prototypes of the: (a) DB-BPF, (b) DB-LNA, (c) Co-design DB-LNA, and DB-BPF. The DB-BPF occupied 3.8 × 2.1 cm or 7.98 cm^2, and the DB-LNA

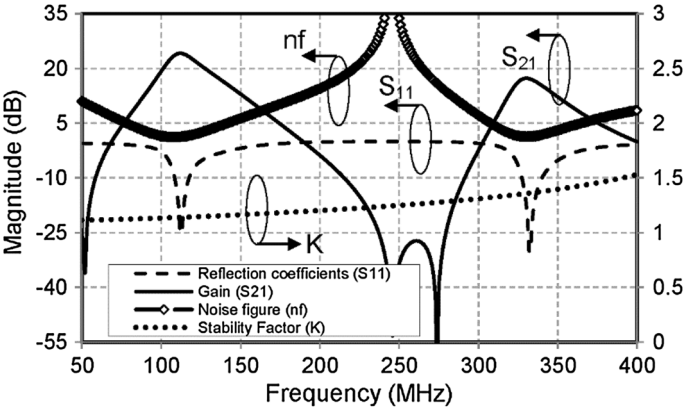

Fig. 23 The simulation result of the S_{11} (dB), gain S_{21} (dB), nf, and K of the co-design structure of the DB-LNA and DB-BPF

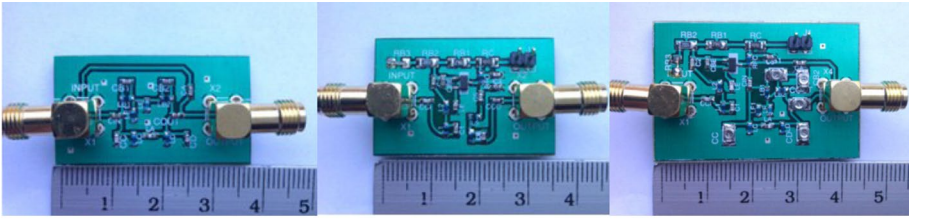

Fig. 24 Fabricated **a** DB-BPF [Model-1], **b** DB-LNA [Model-2], **c** Co-design DB-LNA and DB-BPF[Model-4]

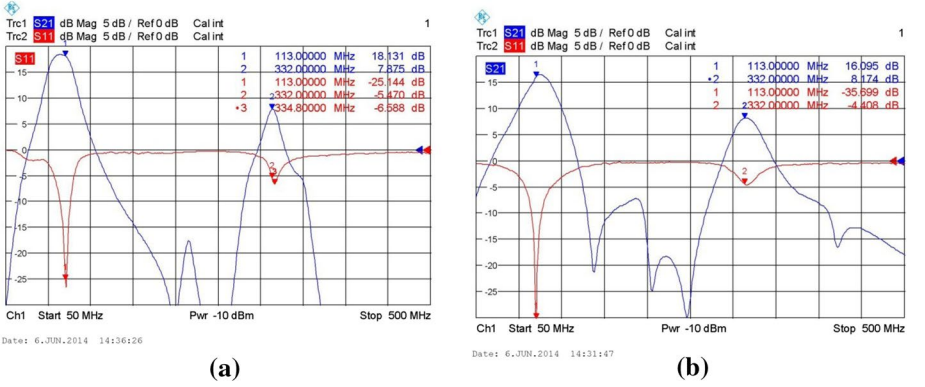

Fig. 25 The S_{11} and S_{21} performance results of the measured **a** Cascade DB-LNA and DB-BPF, **b** Co-design DB-LNA and DB-BPF

occupied 3.7×2.1 cm or 7.77 cm^2. Consequently, the total size of the cascade DB-LNA and DB-BPF was 15.75 cm^2. Furthermore, the total size of the co-design DB-LNA and DB-BPF was 4.5×3.1 cm or 13.95 cm^2. Figure 25a, b show the S_{11} and S_{21} performances

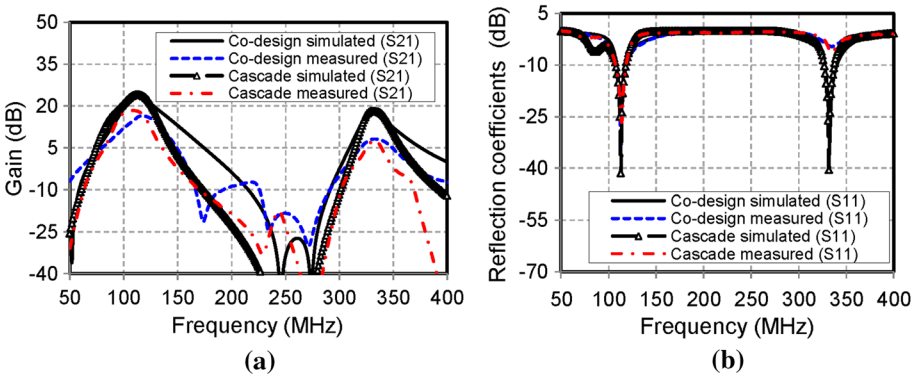

Fig. 26 Comparison between the simulated and measured **a** gain and **b** reflection coefficients

Table 1 Comparison of the results of the cascade method and the co-design method

Parameters	Cascade DB-LNA and DB-BPF				Co-design DB-LNA and DB-BPF			
	$f_1 = 113$ MHz		$f_2 = 332$ MHz		$f_1 = 113$ MHz		$f_2 = 332$ MHz	
	Sim	Meas	Sim	Meas	Sim	Meas	Sim	Meas
Gain (dB)	24.11	18.31	18.11	7.85	24.11	16.08	17.21	8.19
Bandwidth − 3 dB (MHz)	23	26	11	15	20	30	22	30
Noise figure (dB)	1.24	1.24*	1.25	1.25*	1.28	1.28*	1.25	1.28*
Stability factor (K)	1.14	1.14*	1.36	1.36*	1.15	1.15*	1.77	1.15*
V_{CC} (V)	12				12			
Power (mW)	20				20			
Output passive component (Output matching network and DB-BPF)	19				13 component reduction (31.5%)			
Total circuit size (cm^2)	15.75 cm^2				13.96 cm^2 size reduction (11.36%)			

*Simulated result

of the measured cascade DB LNA and DB BPF and the co-design DB LNA and DB BPF, respectively.

The validity of the proposed method was confirmed by the good agreement between the results of the simulation and measurement at a frequency of 113 MHz and 332 MHz, as shown in Fig. 26. The results of the cascaded DB-LNA and DB-BPF reflected by S_{21}, nf, K, BW were 24.11 dB, 1.24 dB, 1.14, 23 MHz, respectively at 113 MHz, and 18.11 dB, 1.25 dB, 1.36, 11 MHz, respectively at 332 MHz. Moreover, the results of the LNA-Filter with the co-design DB-LNA and DB-BPF reflected by S_{21}, nf, K, BW were 24.11 dB, 1.28 dB, 1.15, 20 MHz, respectively, at 113 MHz, and 17.21 dB, 1.25 dB, 1.77, 22 MHz, respectively, at 332 MHz. These results showed that the co-design and cascade structures had nearly the same performance; however, the co-design structure had the advantage of reducing the number of passive components, along with being of a smaller size.

Table 1 shows the comparison results of the cascade and co-design DB LNA and DB BPF. The contributions of this paper included showing that: (1) the co-design method reduced the passive components by 31.5%, (2) the size of the DB-LNA and DB-BPF using

Table 2 Performance comparison on figure of merit (FoM)

Ref.	Single/ dual band	Gain (dB)	nf (dB)	Power (mW)	FoM
Cascade DB-LNA and DB-BPF [Proposed]	f_1	18.31	1.24*	20.00	3.81
	f_2	7.85	1.25*	20.00	1.57
Co-design DB-LNA and DB-BPF [Proposed]	f_1	16.08	1.28*	20.00	2.87
	f_2	8.19	1.25*	20.00	1.64
[19]	f	10.70	5.60	12.10	0.19
[21]	f	21.20	2.50	7.20	1.96
[22]	f	18.00	8.50	40.00	0.06
[23]	f	21.00	2.00	7.05	2.98
[27]	f_1	18.00	1.98	10.00	1.84
	f_2	15.20	1.95	10.00	1.60

*Simulated result

the co-design method size was smaller than the cascaded method by 11.36%, and (3) it was more light-weight in implementation. The validity of this method was evidenced by the good agreement between the simulated and measured results. Finally, it is shown from Table 2 that the FoM of the proposed DB-LNA design methods are higher than that of another LNA.

5 Conclusions

A co-design of the DB-LNA with DB-BPF as the output matching network (OMN) was proposed. To reduce the circuit components, the DB-LNA was directly integrated with the DB-BPF, instead connecting the OMN of the DB-LNA to the 50 Ω-port of the DB-BPF. Consequently, this DB-BPF had a double function, working not only as the DB-BPF but also as the OMN. This proposed method was applied to an RNA communication. Furthermore, the validity of the proposed method was confirmed by good agreement between the simulation and measurement results at frequencies of 113 MHz and 332 MHz.

Acknowledgements The authors say many thanks to the Indonesian Academy of Sciences (LIPI) Bandung for their contribution in fabricating the devices and evaluating the performance of the proposed devices.

Author Contributions All the authors contributed to the paper. The conceptualization, G.W. and M.W.; methodology, M.W.; validation, M.W., J.W., and E.W.; writing—original draft preparation, T.F., and G.W.; writing—review and editing, G.W.; supervision, G.W.; funding acquisition, G.W.

Funding This research is supported by the Directorate of Research and Community Service at Universitas Indonesia through Grant of International Indexed Publication (PUTI) 2020, with contract number NKB-2490/UN2.RST/HKP.05.00/2020.

Compliance with Ethical Standards

Conflict of interest The authors declare no conflict of interest.

References

1. Sim, C. Y. D., Shih, Y. K., & Chang, M. H. (2015). Compact slot antenna for wireless local area network 2.4/5.2/5.8 GHz applications. *IET Microwaves, Antennas and Propagation, 9*(6), 495–501. https://doi.org/10.1049/iet-map.2013.0688.
2. Yang, C. W., & Jung, C. W. (2010). Broad dual-band PIFA using self-complementary structure for DVB-H applications. *Electronics Letters, 46*(9), 606–608. https://doi.org/10.1049/el.2010.0512.
3. Sattar, S., Zainal, T. U. N., & Zulkifli, A. (2017). A 2. 4/5. 2-GHz concurrent dual-band CMOS low noise amplifier. *IEEE Access, 5,* 2148–21156. https://doi.org/10.1109/ACCESS.2017.2756985.
4. Firmansyah, T., et al. (2017). Dual-wideband band pass filter using folded cross-stub stepped impedance resonator. *Microwave and Optical Technology Letters, 59*(11), 2929–2934. https://doi.org/10.1002/mop.30848.
5. Qi, G., Mak, P. I., & Martins, R. P. (2017). A 0.038-mm2 SAW-less multiband transceiver using an N-Path SC gain loop. *IEEE Journal of Solid-State Circuits, 52*(8), 2055–2070. https://doi.org/10.1109/JSSC.2017.2697409.
6. Farazian, M., Asuri, B., & Larson, L. E. (2010). A dual-band CMOS CDMA transmitter without external SAW filtering. *IEEE Transactions on Microwave Theory and Techniques, 58*(5 PART 2), 1349–1358. https://doi.org/10.1109/tmtt.2010.2042851.
7. Maeda, T., et al. (2006). A low-power dual-band triple-mode WLAN CMOS transceiver. *IEEE Journal of Solid-State Circuits, 41*(11), 2481–2489. https://doi.org/10.1109/JSSC.2006.883323.
8. Chang, W. S., & Chang, C. Y. (2011). Analytical design of microstrip short-circuit terminated stepped-impedance resonator dual-band filters. *IEEE Transactions on Microwave Theory and Techniques, 59*(7), 1730–1739. https://doi.org/10.1109/TMTT.2011.2132140.
9. Le Dai, G., Guo, Y. X., & Xia, M. Y. (2010). Dual-band bandpass filter using parallel short-ended feed scheme. *IEEE Microwave and Wireless Components Letters, 20*(6), 325–327. https://doi.org/10.1109/LMWC.2010.2047517.
10. Tseng, C. H., & Shao, H. Y. (2010). A new dual-band microstrip bandpass filter using net-type resonators. *IEEE Microwave and Wireless Components Letters, 20*(4), 196–198. https://doi.org/10.1109/LMWC.2010.2042549.
11. Liu, H. W., et al. (2010). Compact dual-band bandpass filter using defected microstrip structure for GPS and WLAN applications. *Electronics Letters, 46*(21), 1444–1445. https://doi.org/10.1049/el.2010.2146.
12. Hung, C.-Y., Yang, R.-Y., & Lin, Y.-L. (2010). A simple method to design a compact and high performance dual-band bandpass filter for GSM and WLAN. *Progress in Electromagnetics Research C, 13,* 187–193.
13. Chen, X., Han, G., Ma, R., Gao, J., & Zhang, W. (2009). Design of balanced dual-band bandpass filter with self-feedback structure. *ETRI Journal, 31*(4), 475–477. https://doi.org/10.4218/etrij.09.0209.0062.
14. Weng, M. H., Wu, H. W., & Su, Y. K. (2007). Compact and low loss dual-band bandpass filter using pseudo-interdigital stepped impedance resonators for WLANs. *IEEE Microwave and Wireless Components Letters, 17*(3), 187–189. https://doi.org/10.1109/LMWC.2006.890463.
15. Mingqi, Z., Xiaohong, T., & Fei, X. (2008). Compact dual band bandpass filter using novel E-type resonators with controllable bandwidths. *IEEE Microwave and Wireless Components Letters, 18*(12), 779–781. https://doi.org/10.1109/LMWC.2008.2007696.
16. Wu, B., Liang, C. H., Li, Q., & Qin, P. Y. (2008). Novel dual-band filter incorporating defected SIR and microstrip SIR. *IEEE Microwave and Wireless Components Letters, 18*(6), 392–394. https://doi.org/10.1109/LMWC.2008.922614.
17. Lin, Y. C., Horng, T. S., & Huang, H. H. (2014). Synthesizing a multiband LTCC bandpass filter with specified transmission- and reflection-zero frequencies. *IEEE Transactions on Microwave Theory and Techniques, 62*(12), 3351–3361. https://doi.org/10.1109/TMTT.2014.2365454.
18. Qin, P., & Xue, Q. (2017). Compact wideband LNA with gain and input matching bandwidth extensions by transformer. *IEEE Microwave and Wireless Components Letters, 27*(7), 657–659. https://doi.org/10.1109/LMWC.2017.2711524.
19. Qin, P., & Xue, Q. (2017). Design of wideband LNA employing cascaded complimentary common gate and common source stages. *IEEE Microwave and Wireless Components Letters, 27*(6), 587–589. https://doi.org/10.1109/LMWC.2017.2701300.
20. Belmas, F., Hameau, F., & Fournier, J. (2012). A low power inductorless wideband LNA with Gm enhancement and noise cancellation. *IEEE Microwave and Wireless Components Letters, 47*(5), 1094–1103. https://doi.org/10.1109/JSSC.2012.2185533.

21. Singh, R., Slovin, G., Xu, M., Schlesinger, T. E., Bain, J. A., & Paramesh, J. (2017). A reconfigurable dual-frequency narrowband CMOS LNA using phase-change RF Switches. *IEEE Transactions on Microwave Theory and Techniques, 65*(11), 4689–4702. https://doi.org/10.1109/TMTT.2017.2742481.
22. Ulusoy, A. Ç., Kaynak, M., Purtova, T., Tillack, B., & Schumacher, H. (2012). 24 to 79 GHz frequency band reconfigurable LNA. *Electronics Letters, 48*(25), 1598–1600. https://doi.org/10.1049/el.2012.2830.
23. Wibisono, G., & Firmansyah, T. (2012). Concurrent multiband low noise amplifier with multisection impedance transformer. In *Asia-Pacific Microwave Conference Proceedings, APMC*, 2012, https://doi.org/10.1109/apmc.2012.6421776.
24. Wu, W. J., Liu, Q. F., Zhang, Q., & Deng, J. Y. (2013). Co-design of a compact dual-band filter-antenna for WLAN application. *Progress in Electromagnetics Research, 40*(May), 129–139. https://doi.org/10.2528/PIERL13030411.
25. Zhang, B., Zhang, W., Runbo, M., Zhang, X., & Mao, J. (2008). A co-design study of filters and oscillator for low phase noise and high harmonic rejection. *ETRI Journal, 30*(2), 344–346. https://doi.org/10.4218/etrij.08.0207.0292.
26. Oraizi, H., & Esfahlan, M. S. (2010). Optimum design of lumped filters incorporating impedance matching by the method of least squares. *Progress in Electromagnetics Research, 100,* 83–103. https://doi.org/10.2528/PIER09111611.
27. Ma, R., & Zhang, W. (2010). Co-design of dual-band low noise amplifier and band-pass filter. *Asia-Pacific Symposium on Electromagnetic Compatibility, APEMC, 2010,* 1378–1380. https://doi.org/10.1109/APEMC.2010.5475589.
28. Joshi, H., & Chappell, W. J. (2006). Dual-band lumped-element bandpass filter. *IEEE Transactions on Microwave Theory and Techniques, 54*(12), 4169–4177.

Gunawan Wibisono (M'94) received the B.Eng. degree in electrical engineering from the University of Indonesia, Depok, Indonesia, in 1990, and the M.Eng. and Ph.D. degrees from Keio University, Japan, in 1995 and 1998, respectively. He is a former Head of the Electrical Engineering Department, University of Indonesia. His research interests include coding and wireless communications, optical communications, and telecommunication regulation.

Muh Wildan was born in Purworejo, Indonesia. He received B.Eng (S.T) degree in electrical engineering from the University of Borneo, Tarakan, Indonesia, in 2007 and M.Eng (M.T) degree in telecommunication engineering from Department of Electrical Engineering of the University of Indonesia in 2014 respectively. In 1998 he joined in Juwata International Airport as an air telecommunication and navigation technician, In 2008 he moved his job to center of laboratory in Aviation Engineering Division as an air navigation engineer. In 2018, he joined the Air Navigation Engineering Technology, Department of Aviation Engineering, Sekolah Tinggi Penerbangan Indonesia as a researcher and lecturer. His research interests include radio frequency circuit and antenna for aviation applications.

Johan Wahyudi was born in Pasuruan, Indonesia, He received Diploma 3 (A.Md) Degree in Air Navigation Technical Engineering from Pendidikan dan Latihan Penerbangan Curug, he received B. Ed (S.Pd) degree in language and Art from Universitas Borneo Tarakan, Diploma 4 (S.ST) Degree in Navigation Technical Engineering from Sekolah Tinggi Penerbangan Indonesia and M. Eng (M.T) degree in Transportation Engineering from Universitas Brawijaya in 1999, 2010, 2013 and 2016, respectively. In 2000 he joined in Juwata International Airport as an air telecommunication and navigation technician, In 2014 he moved his job to Arinav Indonesia as an air telecommunication and navigation engineer. And since in 2017 he joined in Departement of Aviation Engineering Sekolah Tinggi Penerbangan Indonesia as an instructor and researcher.

Ego Widoro was born in Jakarta, Indonesia. He received B.Eng (S.T) degree in mechanical engineering from Universitas Mercu Buana, Diploma 4 in Aircraft Maintenance Engineering (S.SiT) from Sekolah Tinggi Penerbangan Indonesia and M.Eng (M.T) degree in Industrial engineering from Universitas Mercu Buana in 2007, 2010 and 2015, respectively. In 2002, he joined the Department of Aviation Engineering Sekolah Tinggi Penerbangan Indonesia and since 2011 was start as a researcher and lecturer.

Teguh Firmansyah was born in Subang, Indonesia. He received the B.Eng. (S.T.) degree in electrical engineering and the M.Eng. (M.T.) degree in telecommunication engineering from the Department of Electrical Engineering, Universitas Indonesia, in 2010 and 2012, respectively. Now, he is currently pursuing the Ph.D degree in electrical engineering at Universitas Indonesia and Shizuoka University with double-degree program. In 2012, he joined the Department of Electrical Engineering, Universitas Sultan Ageng Tirtayasa, as a Researcher and a Lecturer. He has authored or coauthored over 25 articles published in refereed journals and conferences. He holds two patents for wideband antenna and multiband antenna. His research interests include microstrip antenna and microwave circuit for various applications. He is a member of the IEEE Antenna and Propagation Society (AP-S) and the IEEE Microwave Theory and Technique Society (MTT-S). He has been a Reviewer for Electronics Letters (IET), the International Journal of Microwave and Wireless Technologies (Cambridge), the International Journal of Electronics and Communications (Elsevier), Microwave and Optical Technology Letters (Wiley), the International Journal of RF and Microwave Computer-Aided Engineering (Wiley), IEEE Access, and Wireless Personal Communications (Springer).